HHS Public Access

Author manuscript

Adv Ther (Weinh). Author manuscript; available in PMC 2020 October 16.

Published in final edited form as:

Adv Ther (Weinh). 2019 August ; 2(8): . doi:10.1002/adtp.201900046.

Targeted Delivery of an siRNA/PNA Hybrid Nanocomplex Reverses Carbon Tetrachloride-Induced Liver Fibrosis

Akshay Jain, **Ashutosh Barve**, **Zhen Zhao**, **John Peter Fetse**, **Hao Liu**, **Yuanke Li**, **Kun Cheng***

Division of Pharmacology and Pharmaceutical Sciences, School of Pharmacy, University of Missouri-Kansas City, Kansas City, MO 64108, USA

Abstract

Liver fibrosis is a wound healing process with excessive accumulation of extracellular matrix in the liver. We recently discovered a PCBP2 siRNA that reverses fibrogenesis in activated hepatic stellate cells (HSCs), which are the key players in liver fibrogenesis. However, targeted delivery of siRNAs to HSCs still remains a challenge. Herein, we developed a new strategy to fabricate a multicomponent nanocomplex using siRNA/PNA hybrid instead of chemically conjugated siRNA, thus increasing the scalability and feasibility of the siRNA nanocomplex for animal studies. We modified the nanocomplex with an insulin growth factor 2 receptor (IGF2R)-specific peptide, which specifically binds to activated HSCs. The siRNA nanocomplex shows a controllable size and high serum stability. The nanocomplex also demonstrates high cellular uptake in activated HSCs *in vitro* and *in vivo*. Anti-fibrotic activity of the siRNA nanocomplex was evaluated in rats with carbon tetrachloride-induced liver fibrosis. Treatment with the PCBP2 siRNA nanocomplex significantly inhibits the mRNA expressions of PCBP2 and type I collagen in fibrotic liver. Histology study revealed that the siRNA nanocomplex efficiently reduces the protein level of type I collagen and reverses liver fibrosis. Our data suggest that the nanocomplex efficiently delivers the siRNA to fibrotic liver and produces a potent anti-fibrotic effect.

Graphical Abstract

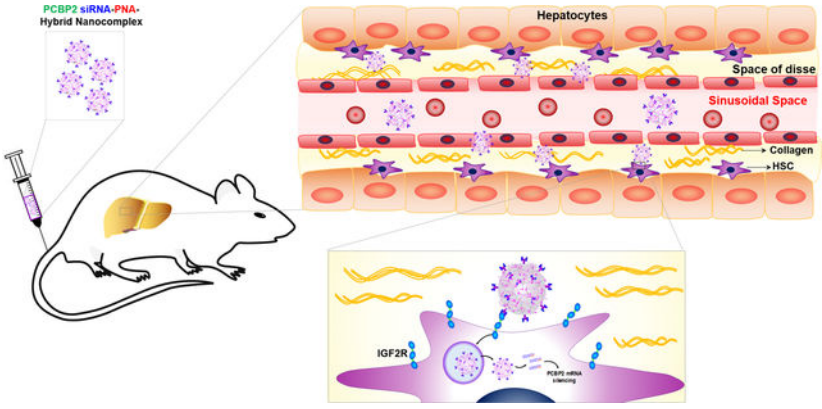

*Corresponding author: Kun Cheng, Ph.D., Professor, Division of Pharmacology and Pharmaceutical Sciences, School of Pharmacy, University of Missouri-Kansas City, 2464 Charlotte Street, Kansas City, MO 64108, Phone: (816) 235-2425 Fax: (816) 235-5779, chengkun@umkc.du.

Keywords

Nanocomplex; peptide nucleic acid; siRNA; liver fibrosis; IGF2R; PCBP2; peptide ligand

Introduction

Liver fibrosis is a wound healing process with excessive accumulation of extracellular matrix (ECM) in the liver after chronic liver injuries, such as nonalcoholic fatty liver disease (NAFLD), nonalcoholic steatohepatitis (NASH), cholestasis, hepatitis, and alcohol abuse.[1] Upon chronic liver injuries, hepatocytes produce apoptotic bodies, which are engulfed by the resident Kupffer cells, followed by recruitment of immune cells and activation of hepatic stellate cells (HSCs). Activation of HSCs augments the inflammatory cascade and promotes the synthesis of ECM. Activated HSCs are, therefore, the major contributors to liver fibrosis.[1–2] Despite extensive knowledge of the molecular mechanisms and pathogenesis of liver fibrosis, there is still no standard treatment approved by the Food and Drug Administration (FDA). If left untreated, liver fibrosis may progress to cirrhosis and liver failure. Liver fibrosis and cirrhosis are the major cause of morbidity in developing as well as developed countries. There is an urgent need for a first line therapy that can specifically and effectively alleviates liver fibrosis. Because ECM is accumulated in all types of liver fibrosis, reduction of the accumulated ECM is an effective strategy to treat liver fibrosis regardless of its stimuli.[3]

α-complex protein-2 (encoded by the poly(rC)-binding protein 2 gene, PCBP2) is responsible for the stabilization of type I collagen mRNA, which leads to the accumulation of ECM in fibrotic liver.[4] We recently demonstrated that alcohol and profibrotic cytokines induce the expressions of PCBP2 and type I collagen in HSCs. Subsequently, we discovered a PCBP2 siRNA, which reverses alcohol- and cytokine-induced fibrogenesis in primary rat HSCs and rat HSC cell line HSC-T6.[5] Systemic delivery of siRNAs to activated HSCs in fibrotic liver remains the biggest challenge because of accumulated ECM and low percentage of HSCs in the liver. Previously, we developed a neutravidin-based nanocomplex to deliver biotinylated siRNA to HSCs.[6] However, chemical modification of siRNAs, such as biotinylation, is always difficult and inefficient due to the poor stability of siRNAs. For *in vivo* animal studies and future clinical applications, it is essential to improve this delivery system by increasing drug (siRNA) loading and scalability.

Most recently, we invented a new strategy to non-covalently attach a chemical cargo, such as biotin, to siRNA using peptide nucleic acid (PNA) as a linker.[7] PNAs are oligonucleotide analogues with purine and pyrimidine bases except the phosphodiester backbone is substituted with polyamide. Given the neutral charge, PNAs efficiently anneal with complementary nucleic acids without the repulsion from the negative charge of nucleic acids. PNA also enhances the thermal and enzymatic stability of annealed nucleic acids.[8]

HSCs are the major players in liver fibrogenesis but they only account for a small fraction of total liver cells. As a result, it is essential to fabricate siRNA delivery systems with HSC-specific ligands to specifically deliver anti-fibrotic siRNAs to activated HSCs. A number of molecular targets, such as insulin growth factor 2 receptor (IGF2R), low density lipoprotein

receptor (LDLR), retinol-binding protein (RBPR), platelet-derived growth factor receptor-beata (PDGFR-β), and integrin, have been explored for HSC-specific delivery of anti-fibrotic agents.[9] Among many of the targeting ligands that are specific for these HSC receptors, IGF2R-specific peptide[6b], IGF2R-specific aptamer[10] and Vitamin A (retinol) [11] have shown tremendous promise. Wu et al. recently developed a vitamin A conjugated pH sensitive polymeric micelle for miRNA (miR-29B and miR-122) delivery.[11b] This vitamin A decorated delivery system demonstrated excellent target specificity and produced significant inhibition of CCl_4-induced liver fibrosis in rats. In our previous work, we compared the targeting efficiency of an siRNA nanocomplex modified with vitamin A, IGF2R-specific peptide, and cholesterol.[6b] The IGF2R-specific peptide showed the highest uptake in fibrotic liver and lowest uptake in other organs in a CCl_4-induced rat model. [6b]IGF2R is a glycoprotein that is upregulated in activated HSCs during liver fibrogenesis. [12] As a result, it has been utilized as a target for HSC-specific delivery of anti-fibrotic agents.[13] Using a combinatorial biopanning procedure, we recently discovered a 12-mer IGF2R-specific peptide (peptide-431), which exhibits high affinity to activated HSCs of rat (HSC-T6) and human (LX-2). [12b] Moreover, dimer of the peptide exhibits improved binding affinity in comparison to its monomer counterpart.[12b]

In this study, we utilized biotinylated IGF2R-specific peptide (dimer) as a targeting ligand to deliver the nanocomplex encapsulating the biotinylated-PNA/PCBP2 siRNA hybrid. Various molar ratios of the IGF2R-specific peptide and PCBP2 siRNA were optimized to achieve a high siRNA loading and efficient HSC targeting. The siRNA nanocomplexes were screened for biophysical characteristics, serum stability and *in vitro* cellular uptake. The siRNA nanocomplex with the best *in vitro* performance was further evaluated for *in vivo* anti-fibrotic activity study in rats with CCl_4-induced liver fibrosis.

Material and Methods

Biotin-s-s-PNA (CACCACCAC) was purchased from PNA Bio, Inc. (Newbury Park, CA). The PCBP2 siRNA sense strand with sticky end (5'-GUCAGUGUG GCUCUCUUAUGUGGUGGUGdTdT-3') and the siRNA PCBP2 antisense strand (5'-AUA AGAGAGCCACACUGACdTdT-3') were purchased from GE Healthcare Dharmacon (Lafayette, CO). Neutravidin and CCl_4 were ordered from Fisher Scientific (Hampton, NH). Bioplex assay kit was purchased from Bio-Rad Laboratories (Hercules, CA). Type I Collagen monoclonal antibody and immunohistochemistry kit were obtained from Abcam (Cambridge, MA).

Fabrication and Characterization of the PCBP2 siRNA-PNA Nanocomplex

PCBP2 siRNA duplex with a sticky end was annealed with complementary PNA-s-s-biotin and incubated at 37°C for 30 min to form the PCBP2 siRNA/PNA-biotin hybrid (Figure 1A). A low molecular weight polyethylene glycol (PEG) (1 kDa) was used as a linker between peptide-431 and biotin. The biotin-PEG-peptide-431 was synthesized as described before.[6b] Various molar ratios of PCBP2 siRNA/PNA-biotin : neutravidin : biotin-PEG-peptide-431, such as 2:1:2, 3:1:1, 3.5:1:0.5, 3.8:1:0.2, 3.9:1:0.1 and 3.99:1:0.01 were mixed at room temperature for 10 min to form the siRNA complex, followed by condensation with

protamine at an N/P ratio of 2.5 to form the siRNA nanocomplex with a final siRNA concentration of 100 nM (Figure 1B).

siRNA nanocomplexes diluted in HEPES buffer (pH 7.4) were analyzed for mean particle diameter (nm) and zeta potential (mV) using Malvern Zetasizer Nano-ZS (Malvern Instruments, MA). Morphology of the nanocomplexes was examined with a CM12 transmission electron microscope (TEM) (Philips, Germany) after staining with 1% phosphotungstic acid.

Gel Retardation and Serum Stability

Gel retardation assay was conducted to confirm the annealing of the siRNA/PNA hybrid and the formation of the siRNA nanocomplex. Biotin-conjugated PCBP2 siRNA, PCBP2 siRNA with sticky end, PCBP2 siRNA/PNA-biotin hybrid and the PCBP2 siRNA nanocomplex were analyzed using 20% native poly acrylamide gel electrophoresis (PAGE) at 80V (constant voltage) for 4 h in cold room (4 °C). siRNA was visualized under UV after staining the gel with GelRed. To confirm the release of the PCBP2 siRNA from the nanocomplex, the siRNA/PNA hybrid and nanocomplex were incubated with 40 μM heparin and 100 mM DTT for 10 min to reduce disulfide bond and release free PCBP2 siRNA as described in our previous work.[6a] The Samples were further analyzed by native PAGE as described above.

To evaluate the serum stability, the nanocomplexes were incubated with 50% rat serum at 37 °C for 0 h, 12 h and 24 h. After respective incubation time intervals, samples were incubated with 40 μM heparin and 100 mM DTT for 10 min as described above and then analyzed using the native PAGE.

Surface Plasmon Resonance (SPR)

Binding affinities of the dimeric peptide-431 to recombinant human IGF2R protein (2447-GR, R&D Systems, Minneapolis, MN) and BSA were determined with the BI-4500 SPR system (Biosensing Instrument Inc., Tempe, AZ). HBS-P+ running buffer (pH 7.4) (GE Healthcare, Chicago, IL) was employed at a rate of 60 μL/min. The proteins were immobilization on a CM-5 sensor chip (Biosensing Instrument Inc., Tempe, AZ) as per the company's protocol. Briefly, the chip was activated with the mixture of freshly prepared 0.4 M N-ethyl-N'-dimethylaminocarbodiimide (EDC) and 0.1 M N-hydroxysucciniimide (NHS) (1:1, v/v) at a rate of 60 μL/min for 5 min. IGF2R protein (25 μg/mL) or BSA (1.5 μg/mL) dissolved in acetate buffer (pH 5) was then injected at a rate of 60 μL/min for 3.3 mins. Subsequently, the uncoated chip surface was blocked by 1 M ethanolamine HCl (pH 8.5) at 60 μL/min for 5 min. Finally, 10 μL of 50 mM NaOH was injected three successive times at 60 μL/min to wash off unbound proteins and stabilize the baseline. Protein immobilization levels of about 1000 RU and 3000 RU for IGF2R and BSA proteins, respectively, were obtained. Dimeric peptide-431 solutions were prepared using running buffer at series of dilutions from 2 nM to 5 μM. Binding affinity was calculated by fitting the curve using SPR Data Analysis Version 3.8.4 (Biosensing Instrument Inc., Tempe, AZ).

Binding Affinity of Dimeric Peptide-431 to HSCs

The binding affinities of the dimeric peptide-431 to HSC-T6, HepG2, and MDA-MB-231 cells were measured as previous reported.[12b] The cells were detached using 5 mM EDTA and suspended in PBS at 1×10^6 cells/ml. 5-Fam labeled dimeric peptide-431 at a series of concentrations were incubated with the cells (v/v, 1:1) at 37°C for 60 min under rotation. After centrifugation at 300 g for 10 min, the cells were washed, resuspended in PBS, and subjected to fluorescence analysis using a FACScalibur flow cytometer (BD biosciences, Franklin Lakes, NJ). The data were analyzed using FlowJo™ 10 software (FlowJo, LLC, Ashland, Oregon). The apparent K_D values were calculated using GraphPad Prism.

Cellular Uptake of siRNA Nanocomplexes

Cellular uptake of the nanocomplexes encapsulating Cy5-labeled PCBP2 siRNA was studied by confocal microscopy and flow cytometry as described.[12b, 14] Briefly, HSC-T6 cells were transfected with siRNA nanocomplexes for 1 h and washed with 1 mM heparin containing PBS. The acidic organelles like endosomes and lysosomes in the cells were stained with LysoTracker DND 99, followed by formalin fixation. Disposition of the nanocomplexes inside the cells were examined under a confocal microscope (Leica TCS SP5). To validate the cellular uptake results from confocal microscopy, HSC-T6 cells incubated with nanocomplexes were also detached using non-enzymatic cell dissociation medium and resuspended to detect Cy5-labeled cells using a BD FACS II flow Cytometer (Bectone Dickinson Instruments, Franklin Lakes, NJ).

Biodistribution Study

Liver fibrosis in Sprague Dawley rats was induced with carbon tetrachloride (CCl_4) as described previously and in accordance with the animal research protocol approved by the Institutional Animal Care and Use Committee (IACUC) at the University of Missouri Kansas City. [6a, 10] Briefly, the rats were intraperitoneally injected with the mixture of CCl_4 and olive oil (1:1, v/v) at a dose of 1 μL CCl_4 per gram of body weight in every consecutive third day for 28 days. For *in vivo* biodistribution study, ten rats were randomly divided into 2 groups. Rats in the first group were intravenously (i.v.) administered with Cy5-labeled PCBP2 siRNA (dose: 0.1 mg/kg), and the rats in the second group were i.v. administered with the nanocomplexes (3.5:1:0.5) encapsulating Cy5-labeled siRNA (dose: 0.1 mg/kg). After 2 h, the animals were euthanized, and organs including the liver, lungs, spleen, kidneys and heart were harvested and imaged for fluorescence detection using a Bruker MS FX PRO Imaging System (Billerica, MA). Fluorescence intensity in the region of interest (ROI) was determined using the Bruker molecular imaging software.

Anti-Fibrotic Activity Study in Rats with CCl_4-Induced Liver Fibrosis

Liver fibrosis in Sprague Dawley rats was induced as described above. Anti-fibrotic activity study was conducted in accordance with the protocol approved by the IACUC at the University of Missouri Kansas City. Thirty-two rats were randomized into four groups: healthy control; CCl_4 induction; CCl_4 induction plus treatment with the scrambled siRNA nanocomplex (1 mg/kg); and CCl_4 induction plus treatment with the PCBP2 siRNA nanocomplex (1 mg/kg). The nanocomplexes were formulated either with scrambled siRNA-

PNA or PCBP2 siRNA-PNA at the molar ratio of 3.5:1:0.5. On 14th, 18th, 23rd and 27th day of CCl_4 induction, siRNA nanocomplexes were prepared at a final volume of 200 μL and injected via tail vein. On day 31st, the rats were euthanized, and sera were collected for cytokine assay. Cytokines including IL-1β, IL-4, IL-6, IL-18, TNFα, MCP-1, and RANTES in the serum were detected using the Bio-Plex Pro™ rat cytokine assay kit (Bio-Rad Laboratories, Hercules, CA) as per the company's protocol.

The livers were harvested and cut into two sections, one was frozen in −80 °C for mRNA and protein analysis, and the other one was stored in 4% phosphate buffered formalin for histological analysis. Approximately 25 mg of each liver was homogenized in 500 μL Trizol, and total RNA was extracted as per the company's protocol. Silencing activity of the PCBP2 gene at the mRNA level was determined using real time RT-PCR as we described before.[5b]

Serum ALT and AST Assay

Alanine amino transferase (ALT) assay was performed according to the manufacturer's protocol (Sigma Aldrich, St. Louis, MO). Briefly, 20 μL of serum or pyruvate standards were added to two separate 96 well plates. One hundred microliters of the master mix was added to each well and briefly mixed using a horizontal plate shaker. Initial measurement was taken after 2 minutes ($T_{initial}$) at 570 nm ($A_{initial}$). Plate reader was set at 37±C and measurements were taken every 5 min until 60 mins (T_{final}). Change in absorbance was calculated by subtracting the final absorbance (A_{final}) from the initial absorbance ($A_{initial}$). From the pyruvate standard, concentration of the pyruvate (B) generated in samples from $T_{initial}$ to T_{final}. ALT activity was determined using the following equation: ALT Activity = (B × Sample dilution factor)/(T_{final}-$T_{initial}$) × V. ALT activity value is equivalent to 1.0 nmol of pyruvate generated by the amount of ALT enzyme per minute at 37 °C.

Aspartate amino transferase (AST) assay was performed as per the manufacturer's protocol (BioVision Inc., San Francisco, CA). Briefly, 50 μL (V) of serum samples, positive control and glutamate standards were added to two separate 96 well plates. One hundred microliters of the reaction mix was added to each well and briefly mixed by horizontal plate shaker. Initial measurement was taken after 2 minutes ($T_{initial}$) at 450 nm ($A_{initial}$). Plate reader was set at 37 ±C and measurements were taken kinetically at every 10 min until 60 mins (T_{final}). Change in absorbance was calculated by subtracting final absorbance (A_{final}) from initial absorbance ($A_{initial}$). From the pyruvate standard, concentration of the glutamate (B) generated in samples from $T_{initial}$ to T_{final}. AST activity was calculated using the following equation: AST Activity = (B × Sample dilution factor)/(T_{final}-$T_{initial}$) × V. AST activity value is equivalent to the 1.0 μmol of glutamate generated by the amount of AST enzyme per minute at 37 °C.

Hydroxyproline Assay

Collagen content in the liver was colorimetrically quantified as total hydroxyproline per gram of liver. Briefly, 50 mg of liver tissue was homogenized with 250 μL PBS, transferred to a glass vial containing 500 μL of 12N HCL. The glass vial was tightly capped and hydrolyzed overnight at 120 °C in a dry bath incubator. Using the polyvinylidene fluoride (PVDF) filter, hydrolyzed homogenate was filtered to remove the hydrolyzed tissue residues.

Five microliters of the supernatant or hydroxyproline standard were added to a 96 well plate and gently mixed with 50 μL of citrate/acetate buffer (pH 6.0). Chloramine T (100 μL) was added to each well and mixed gently. After incubation at room temperature for 30 min, DMAB-Ehrlich's reagent (100 μL) was added in each well and incubated at 65°C for 30 min. Absorbance was measured at 550 nm in a microplate reader to calculate total hydroxyproline (μg) per liver weight (mg).

Histological Study

Liver specimens in each group were examined with hematoxylin and eosin (H&E) staining and picro sirius red staining. Briefly, formalin fixed liver tissues were embedded in paraffin and sectioned at thickness of 5 μm and mounted on microscope glass slides. For staining, the respective slides were deparaffinized by three changes of histosol for 5 min, rehydrated by incubation in the series of alcohol (100%, 95%, and 70%) incubation for 1 minute each and finally hydrated with running water for 2 min. To stain the nucleus, rehydrated slides were incubated in the Wiegert's hematoxylin for 30 min followed by washing the slides in running water for 10 min. To stain the collagen in the section, the slides were subjected to the incubation with Picro Sirius Red for 60 min. To differentiate the red stained collagen from other components of tissues and remove the unbound dye, slides were immersed three times in 1% acetic acid, followed by dehydration with 100% alcohol and two changes of histosol before mounting with Cytoseal™ XYL (Richard Allan Scientific™, San Diego, CA)

Immunostaining of Type I Collagen

Dehydrated tissue slides were placed in a boiling citrate buffer (pH 6) for 45 min to expose the epitope from the deep paraffin embedded section. After cooling down the slides with DI water and tris buffered saline (TBS), the tissues were incubated with protein blocking buffer for 1 h, followed by incubation with primary anti-collagen I antibody (rabbit-polyclonal) over night at 4°C. After washing in PBST, the tissue sections were incubated with biotinylated anti-rabbit IgG-HRP secondary antibody for 2 h at room temperature. Streptavidin HRP was sufficiently spread over the tissues followed by color development with Diaminobenzidine (DAB) chromogen. Nuclei in tissue sections were counterstained with Mayer's hematoxylin.

TUNEL Assay

Rehydrated liver tissue sections were fixed with 10% formalin, followed by permeablization with Proteinase K and fixed in formalin again. Further, terminal deoxynucleotidyl transferase (TdT) enzyme catalyzed incorporation of terminal deoxynucleotidyl transferase-EdUTP into broken double-stranded DNA was done for fluorescent detection of apoptotic cells in the tissue sections. Images were captured and analyzed using Leica DMI 3000 B fluorescent microscope and quantified using ImageJ software.

Statistical Analysis

GraphPad Prism 7 software (San Diego, CA) was used for statistical analysis. All data were presented as mean ± SD. Comparison between three or more groups was performed using a

one-way analysis of variance (ANOVA) with Tuckey's Post Hoc test. $P<0.05$ was considered statistically significant.

Results

In our previous study, we incorporated biotin-conjugated PCBP2 siRNA into the neutravidin-based nanocomplexes.[6b] However, chemical modification of siRNAs is always difficult with very low yield. We, therefore, invented a new strategy to non-covalently attach a chemical cargo, such as biotin, to siRNA using PNA as a linker.[7] Herein, we fabricated the siRNA nanocomplexes using the siRNA/PNA-biotin hybrid (Figure 1). We also increased the loading efficiency of the siRNA in the nanocomplex to make it feasible for *in vivo* animal studies. An IGF2R-specific peptide was used as a targeting ligand to enhance the delivery of the nanocomplex to activated HSCs in fibrotic liver.

Characterization of the siRNA Nanocomplexes

Nanocomplexes fabricated with different siRNA/neutravidin/peptide-431 molar ratios were dispersed in HEPES buffer (pH 7.4) and analyzed for particle size and zeta potential. As shown in Figure 2A, both particle size and zeta potential of the nanocomplexes were inversely proportional to the molar ratio of siRNA. Formation of the siRNA nanocomplex is mainly dependent on the electrostatic interaction between negatively charged siRNA and positively charged protamine. High amount of siRNA in the formulation therefore enhances the condensation and subsequently reduces the particles size. Particle size of the nanocomplexes were confirmed with transmission electron microscopy (TEM) (Figure 2B).

Annealing and Serum Stability of PCBP2-siRNA-PNA

The core concept of the siRNA nanocomplex is to non-covalently attach biotin to siRNA using a 9-mer PNA (CACCACCAC) as a linker. Biotin was conjugated to PNA via a disulfide bond, which can be cleaved inside HSCs to release encapsulated siRNA. Ansnealing of the PCBP2 siRNA containing a sticky end at the 3' end of the sense strand with PNA-s-s-biotin was analyzed in 20% native poly acrylamide electrophoresis (PAGE). As illustrated in Figure 2C, PCBP2 siRNA was efficiently annealed with PNA-s-s-biotin and showed retarded migration compared to biotin-conjugated siRNA and siRNA with the stick end. Moreover, PCBP2 siRNA/PNA-s-s-biotin hybrid was completely complexed with the neutravidin nanocomplex and stayed on the interface of the gel. The intensity of the encapsulated siRNA is negligible because of the shielding effect of the nanocomplex.

Release of PCBP2 siRNA from the nanocomplex containing biotin-conjugated siRNA (PCBP2-nano) and nanocomplex containing the siRNA/PNA-s-s-biotin hybrid (PCBP2-PNA-nano) was investigated by incubating the nanocomplexes with 40 μM heparin and 100 mM DTT (Figure 2D). DTT reduces the disulfide linkage, and heparin displaces the siRNA from protamine. Both the PCBP2 siRNA and PCBP2 siRNA/PNA hybrid were successfully released and resolved in the gel. This result suggests that, after cellular uptake by endocytosis, disulfide bond between PCBP2 siRNA/PNA and biotin will be effectively reduced in the acidic environment in endosomes, resulting in the release of PCBP2 siRNA/PNA in the cytoplasm to exert its silencing activity.

Serum stability is one of the biggest barriers for efficient siRNA delivery. After incubation of nanocomplex formulations with different siRNA:neutravidin:peptide-431 molar ratios (3.5:1:0.5, 3.8:1:0.2, 3.9:1:0.1 and 3.99:1:0.1) in 50% rat serum for 0, 12, and 24 h, the mixtures were incubated with 100 mM DTT and 40 μM heparin to release the encapsulated PCBP2 siRNA/PNA hybrid from the nanocomplexes. The mixture was subsequently analyzed using 20% native PAGE (Figure 2E). While free siRNAs were completely degraded in rat serum after 12h, all the nanocomplexes efficiently protect siRNA from degradation in rat serum for up to 12 h. After incubation for 24 h, slight degradation of siRNAs was observed in nanocomplexes with the 3.8:1:0.1, 3.9:1:0.1 and 3.99:1:0.01 molar ratios. By contrast, the nanocomplex with the 3.5:1:0.5 molar ratio protected the siRNA even after 24 h incubation in rat serum.

Binding Affinity of IGF2R-Specific Peptide to IGF2R Protein

Using phage display biopanning, we recently discovered an IGF2R-specific peptide (peptide-431), which can be used as a targeting ligand to deliver various cargoes to activated HSCs [6b, 12b]. Herein, we sought to potentiate the target specificity of the siRNA nanocomplex by incorporating a dimer of peptide-431 in our delivery system. We first compared the affinity of peptide-431 monomer and its dimer toward human IGF2R protein using SPR. As illustrated in Figure 3A and 3B, the equilibrium dissociation constants (K_D) of the monomeric peptide-431 and dimeric peptide-431 for human IGF2R protein are 926 nM and 150 nM, respectively. Moreover, K_D of the dimeric peptide for BSA was 1030 nM (Figure 3B), suggesting not only a high affinity but also a high specificity of the dimeric peptide to IGF2R protein.

We further evaluated the binding affinity and specificity of the dimeric peptide-431 to an activated HSC cell line (HSC-T6), which overexpresses IGF2R.[6b] As revealed in Figure 3D, the dimeric peptide exhibited high affinity to HSC-T6 with an apparent K_D of 79 nM. By comparison, the dimeric peptide showed much lower affinity to a human hepatocellular carcinoma cell line HepG2 (apparent K_D: 806 nM) and a human breast cancer cell line MDA-MB-231 (apparent K_D: 1590 nM). Also, the fluorescence intensity of the dimeric peptide inside HSC-T6 cells is dramatically higher than that in HepG2 and MDA-MB-231 cells (Figure 3E). These data clearly demonstrate the high affinity and specificity of the dimeric peptide to IGF2R on activated HSCs. We subsequently used the dimeric peptide as a targeting ligand in the siRNA nanocomplexes.

Optimization of the Nanocomplex Formulation to Increase siRNA Loading

Nanocomplexes with different siRNA/neutravidin/peptide-431 molar ratios (3.5:1:0.5, 3.8:1:0.2 and 3.9:1:0.1) were examined for cellular uptake in HSCs. All the three nanocomplexes showed 100% uptake in activated HSCs (Figure 4A), but the nanocomplex with the 3.5:1:0.5 ratio showed the highest fluorescence intensity (Figure 4B), suggesting its highest efficiency in delivering siRNAs into HSCs. We also examined cellular uptake using confocal microscopy. After 1 h of incubation with the nanocomplexes, the cells were fixed and imaged under a confocal microscope using the red channel for Cy5-labeled PCBP2 siRNA, green channel for lysotracker, and blue channel for DAPI. In accordance with the flowcytometry data, the nanocomplex with the 3.5:1:0.5 ratio exhibited the highest cellular

uptake in the cells (Figure 4C). Meanwhile, the siRNA loading for the nanocomplex with the 3.5:1:0.5 ratio is approximately 46% (w/w), which is sufficient for animal studies. We, therefore, used the molar ratio 3.5:1:0.5 for the nanocomplex in animal activity study.

Biodistribution of the siRNA Nanocomplexes

Having shown the high cellular uptake of the PCBP2 siRNA nanocomplex in HSCs *in vitro*, we next evaluated its biodistribution in rats with CCl_4-induced liver fibrosis. Cy5-labeled PCBP2 siRNA was annealed with PNA-s-s-biotin and then condensed into the neutravidin-based nanocomplex at the molar ratio of 3.5:1:0.5. In comparison to the free PCBP2 siRNA/PNA hybrid, the siRNA nanocomplex showed 10-fold higher liver uptake (Figure 5). As expected, the free siRNA underwent rapid clearance from the body and showed low fluorescence in most organs. Due to its low molecular weight, the free siRNA was mainly cleared from the kidney and showed higher kidney accumulation compared to the siRNA nanocomplex. This result suggests that the nanocomplex can efficiently protect the siRNA *in vivo* and specifically deliver the siRNA to fibrotic liver.

PCBP2 siRNA Nanocomplex Reverses CCl_4-Induced Liver Fibrosis in Rats

We next sought to determine whether the PCBP2 siRNA nanocomplex reverses CCl_4-induced liver fibrosis in rats. CCl_4 is a xenobiotic that has been widely used to induce chronic liver injury and liver fibrosis in rats.[15] The siRNA nanocomplex was administrated via tail vein at a dose of 1 mg/kg for four times. In the end of the study, the rats were euthanized, and the serum and liver were harvested. We first determined the ALT and AST levels in the serum (Figure 6A and B) to evaluate liver injury caused by CCl_4. In comparison to healthy rats, CCl_4 induction dramatically increased ALT and AST values to 500 IU/L and 464 IU/L, respectively, indicating significant inflammation and damage in the liver. Treatment of the rats with the scrambled siRNA nanocomplex did not reverse the elevated ALT and AST values. By contrast, after treatment with the PCBP2 siRNA nanocomplex, the ALT and AST levels were decreased to 218 IU/L and 215 IU/L, respectively.

We hypothesize that PCBP2 siRNA silences the expression of αCP2 protein and subsequently reduces the accumulated type I collagen in fibrotic liver. We therefore evaluated the expressions of PCBP2 and type I collage at the mRNA level in the liver. As shown in Figure 6C, CCl_4 induction increased the expression of PCBP2 in the liver. This is in accordance with our previous studies that profibrogenic molecules stimulated the expression of PCBP2 in HSCs.[5b] The PCBP2 siRNA nanocomplex efficiently silenced the expression of PCBP2 mRNA in the liver, indicating the nanocomplex can efficiently deliver the siRNA into the liver and exert its silencing activity *in vivo*. We previously demonstrated that silencing PCBP2 in HSCs reduced the half-life of type I collagen mRNA and subsequently downregulated the amount of the mRNA [16]. Herein, we also observed downregulation of type I collagen mRNA in the liver after treatment with the PCBP2 siRNA nanocomplex (Figure 6D). This downregulation is the key for the regression of accumulated ECM in fibrotic liver.

Hydroxyproline is a major component of collagen and comprises approximately 13.5% of total amino acids in collagen. As a result, hydroxyproline assay was performed to determine

the amount of total collagen in the liver (Figure 6E). Compared to healthy rats, CCl_4-treated rats showed escalated hydroxyproline content, indicating extensive accumulation of collagen in the liver. Administration of the scrambled siRNA nanocomplex to CCl_4-treated rats did not reverse the escalated hydroxyproline level. By contrast, the PCBP2 siRNA nanocomplex significantly reduced the amount of hydroxyproline in the livers of CCl_4-treated rats, suggesting a reduction of total collagen in the liver.

To further investigate the anti-fibrotic activity of the siRNA nanocomplex, liver morphology was examined with H&E staining (Figure 7A). Livers from healthy rats showed a normal lobular architecture, while livers from CCl_4-treated rats exhibited significant disruption of the liver architecture and large fibrous septa formation. While treatment with the scrambled siRNA nanocomplex did not improve the morphological changes induced by CCl_4, the PCBP2 siRNA nanocomplex effectively improved the liver morphology of CCl_4-treated rats.

Liver specimen from each group were also stained for collagen fibers by Picro Sirius Red staining, which is one of the most commonly staining methods for collagen type I, III, IV. Picro Sirius Red staining of rats receiving either no treatment or scrambled siRNA treatment exhibited portal-portal and portal-central vein bridging with significant collagenous nodules, indicating severe fibrosis in the liver.[17] While CCl_4 treatment dramatically increased the amount of collagen in the liver, the PCBP2 siRNA nanocomplex substantially reduced the escalated collagen in CCl_4-treated rats. The scrambled siRNA nanocomplex did not alter the expression of collagen in CCl_4-treated rats (Figure 7A&B).

As PCBP2 siRNA specifically downregulated the mRNA of type I collagen, we further examined the protein expression of type I collagen in the liver using immunohistochemistry. As highlighted by arrows in Figure 7A, type I collagen staining was significantly lower in PCBP2 nanocomplex treatment group. Type I collagen positive areas were approximately 8 % of total tissue area in case of the liver fibrosis group, whereas PCBP2 siRNA treated fibrotic rats showed less than 3 % collagen staining (Figure 7C). These results demonstrated significant resolution of type I collagen, which is the main component of accumulated ECM, and amelioration of liver fibrosis after the treatment with the PCBP2 siRNA nanocomplex.

PCBP2 siRNA Nanocomplex Attenuates Hepatocyte Apoptosis

Hepatocyte apoptosis is closely correlated with liver inflammation and fibrosis. Intervention of hepatocyte apoptosis has proven to be beneficial for the resolution of liver fibrosis or liver injury in clinical trials.[18] As indicated in Figure 8A, PCBP2 siRNA treated group showed significantly lower TUNEL positive (apoptotic) cells in comparison to groups receiving either no treatment or scrambled siRNA treatment. We also quantified the TUNEL positive cells from five different areas per slide of five independent samples per group. As shown in Figure 8B, counts for TUNEL positive cells in groups receiving either no treatment or scrambled siRNA treatment were significantly higher than PCBP2 siRNA-treated group. This also supports the assertion derived from literature that regression of apoptosis leads to the resolution of fibrosis and liver injury[18a].

Resolution of Liver Fibrosis Downregulates Proinflammatory Cytokines and Chemokines

We also investigated proinflammatory cytokines in the serum that contribute to liver fibrogenesis. As shown in Figure 9, interleukins (such as IL-1β, IL-4, IL-6 and IL-18) and TNFα were highly elevated in the progression of fibrosis as they govern the proliferation of fibroblasts, T cells and macrophages.[19] After treatment with the PCBP2 siRNA nanocomplex, expressions of the cytokines like IL-1β, IL-4 IL-6 and TNFα were significantly lowered by 2–3 fold in the serum. Levels of IL-18 in PCBP2 siRNA-treated group were found to be lower in some samples, but cumulative expression was statistically insignificant to groups receiving either no treatment or scrambled siRNA. Moreover, profibrogenic chemokines, such as MCP-1 (CCL2) and RANTES (CCL5), promote liver inflammation by interacting with T lymphocytes, monocytes and NK cells.[20] It has been reported that targeting RANTES and MCP-1 helps in amelioration of liver fibrosis.[21] As shown in Figure 9 I and J, MCP-1 and RANTES were significantly downregulated in the rats treated with the PCBP2 siRNA nanocomplex.

Discussion

We previously developed a neutravidin-based nanocomplex to deliver siRNA to HSCs.[6b] While the system showed great promise in delivering siRNA to HSCs *in vivo*, it still faces two major hurdles moving forward to animal activity study. The first limitation is the relatively low drug loading (approximately 10% w/w). We therefore aimed to increase the molar ratio of siRNA in the nanocomplex to increase drug loading (Figure 2), thus minimizing potential side effects associated with the delivery system. By changing the siRNA:neutravidin:peptide molar ratio from 2:1:2 to 3.5:1:0.5 and reducing the N/P ratio from 10 to 5, drug loading of the siRNA nanocomplex was increased to approximately 46% (w/w). Meanwhile, the siRNA nanocomplex with the optimized molar ratio shows a very small particle size (~148 nm), which will be helpful in crossing the liver sinusoids (Figure 2).

Another limitation of the system is the difficulty in chemically conjugating biotin to the siRNA. We recently invented a new strategy to non-covalently attach chemical cargo to siRNAs using PNA as a linker[7], thus avoiding the degradation of siRNAs during chemical conjugation. Annealing of biotinylated PNA to the PCBP2 siRNA is an easy procedure without affecting the activity of the siRNA. As PNAs are extensively stable and resistant to the harsh pH, DNase and RNase, annealing of PNA to an siRNA also helps maintain the stability and potency of the siRNA.[7, 22]

There are several molecular receptor that have been investigated for HSC-targeted delivery, such as low density lipoprotein receptor (LDLR)[16, 23], cellular retinol binding receptor protein 1 (CRBP-1)[24], and IGF2R[25]. We previously demonstrated that IGF2R is a better target compared to CRBP-1 and LDLR. In this study, we further demonstrated that the dimeric peptide-431 has a very high affinity and specificity to IGF2R protein. The dimeric peptide-431 also shows high affinity and specificity to IGF2R-positive HSC-T6 cells, but not to HepG2 and MDA-MB-231 cells (Figure 3). Cellular uptake of the siRNA nanocomplex in HSC-T6 cells is positively correlated with the ratio of the dimeric peptide, indicating the critical role of the peptide ligand in delivering the nanocomplex to HSCs (Figure 4). More

importantly, these results are in concordance with the high liver uptake of the siRNA nanocomplex in the biodistribution study in rats with CCl_4-induced liver fibrosis (Figure 5). In comparison to free siRNA, the nanocomplex showed nearly 10 times higher liver distribution and lower retention in the kidney. Apart from efficient target specificity, small size (148 nm) of the siRNA nanocomplex is supposedly another reason responsible for the optimal extravasation and retention of the therapeutic payload in complex and dense matrix containing tissues.[26]

The main objective of this study is to inhibit the type I collagen production and subsequently reverse liver fibrosis. We hypothesized that after administration, the PCBP2 siRNA nanocomplex will extravasate to the space of Disse and specifically target IGF2R receptors on activated HSCs (Figure 1C). As shown in Figure 6 (D and E), the PCBP2 siRNA nanocomplex suppressed the elevated mRNAs of PCBP2 and type I collagen (Figure 6 D–E). Moreover, the primary serum markers of liver injury such as ALT and AST levels were significantly reduced (Figure 6 A–B). It is noteworthy that the ALT and AST values of the PCBP2 siRNA-treated rats are still slightly higher than that of healthy rats. This could be due to two reasons. Firstly, it could be due to the last injection of CCl_4, which was administered after the last injection of the PCBP2 siRNA. Secondly, we only administered four periodic injections of the PCBP2 siRNA nanocomplex at 1mg/kg. It is possible that we may need a little higher dose or more injections to completely reverse liver fibrosis.

PCBP2 siRNA upon delivery to target cells indirectly suppressed type I collagen production and instigated degradation of accumulated collagen fibers. As highlighted in Figure 6 C, PCBP2 siRNA nanocomplex treated groups showed statistically lower levels of hydroxyproline content in the liver in comparison to the fibrotic rats that received either no treatment or scrambled siRNA. This finding was consistent with the Picro Sirius Red staining and type I collagen immuno-staining results. Moreover, collagen fiber anchoring and bridging were also diminished after treatment with the PCBP2 siRNA nanocomplex, whereas groups receiving no treatment or scrambled siRNA showed advanced fibrotic symptoms with extensive portal-portal and portal-central vein collagen fiber anchorage and bridging with occasional nodules in the liver (Figure 7). Type I collagen has proven to be an efficient target for liver fibrosis therapy. Recently, researchers have developed potential siRNA based therapy targeting type I collagen for liver fibrosis. It is, however, unknown if the regression in type I collagen affects the expression of other collagen fibers. Interestingly, we observed negative regulation of all other collagen fibers after PCBP2 treatment. In one report, Calvente et al. targeted procollagen 1 by siRNA and significantly inhibited the various key collagen fiber production[27] which is consistent with our findings. Other researches have also demonstrated therapeutic suppression of all types of collagen after anti-collagen I siRNA therapy.[28]

HSCs are the primary executioners of liver fibrosis in general and are the principle source of myofibroblast in CCl_4-induced liver fibrosis.[29] They are susceptive of a wide range of molecular signals such as cytokines, chemokines, macrophages and other fibrosis instigator cells that are promoted by hepatocyte apoptosis due to liver injury.[29–30] Moreover, in the presence of proinflammatory cytokines such as TNFα, hepatocytes show enhanced apoptosis.[31] Variable effects of apoptosis on liver fibrosis led us to examine apoptosis in

different treatment groups of liver fibrosis model. TUNEL assay revealed that there was substantial apoptosis across the liver tissue of animals receiving either no treatment or scrambled siRNA treatment (Figure 8A). Interestingly, apoptotic cells (TUNEL positive) were present in a pattern which we believe to be aligned with collagen fiber or scar tissue (Figure 7). It can be postulated that the cells near the collagen matrix and scar tissue were exposed to more resistance, hypoxia and CCl_4, resulting in significant apoptosis and scaring. Such tissue damage and consequent activation of HSCs result in collagen fiber deposition across hepatic vasculature and liver tissue. PCBP2 siRNA treatment group showed significantly lower apoptotic cells which are responsible for perpetual signaling to maintain the activation of HSCs. Similarly, several other groups also reported the reduction in hepatocyte apoptosis after liver fibrosis therapy.[32]

Hepatic inflammation is closely associated with apoptotic bodies, cytokines and chemokines[33]. Autocrine signals from inflammatory cells or activated HSCs reinforce the survival and maintenance of activated HSCs.[34] Since inflammation is a critical factor that governs HSC activation and fibrogenesis, many efforts have been devoted to evaluating the effect of fibrosis therapy on inflammation.[35] It has been reported that cytokines such as TGF β 1, interleukins and PDGF are often elevated in fibrotic rats, and their expressions are dramatically lowered upon the regression of liver fibrosis.[36] Therefore, we investigated serum from the respective treatment and control groups for changes in cytokines (IL-1β, IL-6, IL-18 and TNFα) that regulate liver fibrogenesis. As IL-1β, IL-6, and TNFα are highly overexpressed in the patients with advanced liver fibrosis, cirrhosis and hepatitis, they are, therefore, considered important serum markers to measure clinical outcome.[37] These cytokines directly or indirectly promote the survival and activation of HSCs during liver fibrogenesis. Furthermore, chemokines such as MCP-1 (CCL2) and RANTES (CCL5) are considered potential profibrogenic factors because of their involvement in liver injury, HSC recruitment and activation.[34] Both MCP-1 and RANTES were found to be highly expressed in animals with CCl_4-induced liver fibrosis.[34, 38]

Taken together, we invented a highly specific and efficient therapeutic delivery system for siRNA. As simple as it is in its fundamental concept, IGF2R targeted PCBP2 siRNA nanocomplex is as potent in reversal of fibrosis progression and inhibition of type I collagen in CCl_4-induced liver fibrosis model. Efficient delivery of PCBP2 siRNA to the liver not only resolved fibrosis but functionally restored the liver by significantly reducing the molecular serum markers such as ALT, AST, proinflammatory cytokines and chemokines. The PCBP2 siRNA nanocomplex holds a great promise for liver fibrosis therapy.

Supplementary Material

Refer to Web version on PubMed Central for supplementary material.

Acknowledgements

This work is supported by the award (2R01AA021510) from the National Institutes of Health. Part of the work is supported by an AAPS Foundation Graduate Student Fellowship awarded to Akshay Jain.

References

[1]. Cohen-Naftaly M, Friedman SL, Therap Adv Gastroenterol 2011, 4, 391.

[2]. Cheng K, Mahato RI, Crit Rev Ther Drug Carrier Syst 2007, 24, 93. [PubMed: 17725523]

[3]. a)Friedman SL, Nature Biotechnology 2008, 26, 399;b)Sato Y, Murase K, Kato J, Kobune M, Sato T, Kawano Y, Takimoto R, Takada K, Miyanishi K, Matsunaga T, Takayama T, Niitsu Y, Nat Biotechnol 2008, 26, 431. [PubMed: 18376398]

[4]. Lindquist JN, Parsons CJ, Stefanovic B, Brenner DA, J Biol Chem 2004, 279, 23822. [PubMed: 14973140]

[5]. a)Shukla RS, Qin B, Wan YJ, Cheng, Pharm Res 2011, 28, 3058; [PubMed: 21643860] b)Liu H, Chen Z, Jin W, Barve A, Wan YY, Cheng K, Liver Res 2017, 1, 70. [PubMed: 28966795]

[6]. a)Jain A, Barve A, Zhao Z, Jin W, Cheng K, Mol Pharm 2017, 14, 1517; [PubMed: 28026957] b)Zhao Z, Li Y, Jain A, Chen Z, Liu H, Jin W, Cheng K, Nanomedicine 2018, 14, 51. [PubMed: 28890106]

[7]. Jin W, Jain A, Liu H, Zhao Z, Cheng K, ACS Applied Bio Materials 2018, 1, 643.

[8]. a)Pellestor F, Paulasova P, Eur J Hum Genet 2004, 12, 694; [PubMed: 15213706] b)Ura Y, Beierle JM, Leman LJ, Orgel LE, Ghadiri MR, Science 2009, 325, 73. [PubMed: 19520909]

[9]. Chen Z, Jain A, Liu H, Zhao Z, Cheng K, J Pharmacol Exp Ther 2019, DOI: 10.1124/jpet.118.256156.

[10]. Chen Z, Liu H, Jain A, Zhang L, Liu C, Cheng K, Theranostics 2017, 7, 2982. [PubMed: 28839458]

[11]. a)Zhang Z, Wang C, Zha Y, Hu W, Gao Z, Zang Y, Chen J, Zhang J, Dong L, ACS Nano 2015, 9, 2405; [PubMed: 25587629] b)Wu J, Huang J, Kuang S, Chen J, Li X, Chen B, Wang J, Cheng D, Shuai X, Adv Sci (Weinh) 2019, 6, 1801809. [PubMed: 30886803]

[12]. a)de Bleser PJ, Jannes P, van Buul-Offers SC, Hoogerbrugge CM, van Schravendijk CF, Niki T, Rogiers V, van den Brande JL, Wisse E, Geerts A, Hepatology 1995, 21, 1429; [PubMed: 7737649] b)Chen Z, Jin W, Liu H, Zhao Z, Cheng K, Mol Pharm 2015, 12, 2180. [PubMed: 25955351]

[13]. Ye Z, Cheng K, Guntaka RV, Mahato RI, Bioconjug Chem 2006, 17, 823. [PubMed: 16704223]

[14]. Qin B, Chen Z, Jin W, Cheng K, J Control Release 2013, 172, 159. [PubMed: 23968830]

[15]. a)Scholten D, Trebicka J, Liedtke C, Weiskirchen R, Lab Anim 2015, 49, 4; [PubMed: 25835733] b)Moraru L, Moldovanu S, Culea-Florescu AL, Bibicu D, Ashour AS, Dey N, Microsc Res Tech 2017, 80, 862. [PubMed: 28370776]

[16]. Shukla RS, Jain A, Zhao Z, Cheng K, Nanomedicine 2016, 12, 1323. [PubMed: 26970028]

[17]. Goodman ZD, J Hepatol 2007, 47, 598. [PubMed: 17692984]

[18]. a)Wang, Cell Death Dis 2014, 5, e996; [PubMed: 24434519] b)Guicciardi ME, Gores GJ, Gut 2005, 54, 1024. [PubMed: 15951554]

[19]. b)Borthwick LA, Wynn TA, Fisher AJ, Biochim Biophys Acta 2013, 1832, 1049; [PubMed: 23046809] b)Tsukamoto H, Alcohol Clin Exp Res 1999, 23, 911. [PubMed: 10371413]

[20]. a)Sadeghi M, Lahdou I, Oweira H, Daniel V, Terness P, Schmidt J, Weiss KH, Longerich T, Schemmer P, Opelz G, Mehrabi A, Br J Cancer 2015, 113, 756; [PubMed: 26270232] b)Elsabahy M, Wooley KL, Chem Soc Rev 2013, 42, 5552; [PubMed: 23549679] c)Farci P, Wollenberg K, Diaz G, Engle RE, Lai ME, Klenerman P, Purcell RH, Pybus OG, Alter HJ, Proc Natl Acad Sci U S A 2012, 109, 14562. [PubMed: 22829669]

[21]. Berres ML, Koenen RR, Rueland A, Zaldivar MM, Heinrichs D, Sahin H, Schmitz P, Streetz KL, Berg T, Gassler N, Weiskirchen R, Proudfoot A, Weber C, Trautwein C, Wasmuth HE, J Clin Invest 2010, 120, 4129. [PubMed: 20978355]

[22]. a)Deleavey GF, Damha MJ, Chem Biol 2012, 19, 937; [PubMed: 22921062] b)Oh SY, Ju Y, Park H, Mol Cells 2009, 28, 341. [PubMed: 19812898]

[23]. Lytle KA, Depner CM, Wong CP, Jump DB, J Lipid Res 2015, 56, 1936. [PubMed: 26315048]

[24]. a)Lee H, Jeong H, Park S, Yoo W, Choi S, Choi K, Lee MG, Lee M, Cha D, Kim YS, Han J, Kim W, Park SH, Oh J, EMBO Mol Med 2015, 7, 819; [PubMed: 25864124] b)Furuhashi H, Tomita K, Teratani T, Shimizu M, Nishikawa M, Higashiyama M, Takajo T, Shirakabe K, Maruta K,

Okada Y, Kurihara C, Watanabe C, Komoto S, Aosasa S, Nagao S, Yamamoto J, Miura S, Hokari R, Hepatol Res 2018, 48, 397. [PubMed: 29243365]

[25]. a)Yang N, Singh S, Mahato RI, J Control Release 2011, 155, 326; [PubMed: 21763370] b)Adrian JE, Poelstra K, Scherphof GL, Molema G, Meijer DK, Reker-Smit C, Morselt HW, Kamps JA, J Hepatol 2006, 44, 560. [PubMed: 16368158]

[26]. Brigger I, Dubernet C, Couvreur P, Adv Drug Deliv Rev 2002, 54, 631. [PubMed: 12204596]

[27]. Jimenez Calvente C, Sehgal A, Popov Y, Kim YO, Zevallos V, Sahin U, Diken M, Schuppan D, Hepatology 2015, 62, 1285. [PubMed: 26096209]

[28]. Vollmann EH, Cao L, Amatucci A, Reynolds T, Hamann S, Dalkilic-Liddle I, Cameron TO, Hossbach M, Kauffman KJ, Mir FF, Anderson DG, Novobrantseva T, Koteliansky V, Kisseleva T, Brenner D, Duffield J, Burkly LC, Mol Ther Nucleic Acids 2017, 7, 314. [PubMed: 28624207]

[29]. Mederacke I, Hsu CC, Troeger JS, Huebener P, Mu X, Dapito DH, Pradere JP, Schwabe RF, Nat Commun 2013, 4, 2823. [PubMed: 24264436]

[30]. a)Pradere JP, Kluwe J, De Minicis S, Jiao JJ, Gwak GY, Dapito DH, Jang MK, Guenther ND, Mederacke I, Friedman R, Dragomir AC, Aloman C, Schwabe RF, Hepatology 2013, 58, 1461; [PubMed: 23553591] b)Ding BS, Cao Z, Lis R, Nolan DJ, Guo, Simons M, Penfold ME, Shido K, Rabbany SY, Rafii S, Nature 2014, 505, 97. [PubMed: 24256728]

[31]. Liu M, Mendicino M, Ning Q, Ghanekar A, He W, McGilvray I, Shalev I, Pivato D, Clark DA, Phillips MJ, Levy GA, J Immunol 2006, 176, 7028. [PubMed: 16709865]

[32]. a)Friedman SL, Physiol Rev 2008, 88, 125; [PubMed: 18195085] b)Zhang K, Han X, Zhang Z, Zheng L, Hu Z, Yao Q, Cui H, Shu G, Si M, Li C, Shi Z, Chen T, Han Y, Chang Y, Yao Z, Han T, Hong W, Nat Commun 2017, 8, 144. [PubMed: 28747678]

[33]. Czaja AJ, World J Gastroenterol 2014, 20, 2515. [PubMed: 24627588]

[34]. Seki E, Schwabe RF, Hepatology 2015, 61, 1066. [PubMed: 25066777]

[35]. Koyama Y, Brenner DA, J Clin Invest 2017, 127, 55. [PubMed: 28045404]

[36]. a)Cheng K, Yang N, Mahato RI, Mol Pharm 2009, 6, 772; [PubMed: 19388665] b)Czochra P, Klopcic B, Meyer E, Herkel J, Garcia-Lazaro JF, Thieringer F, Schirmacher P, Biesterfeld S, Galle PR, Lohse AW, Kanzler, J Hepatol 2006, 45, 419; [PubMed: 16842882] c)Dooley S, ten Dijke P, Cell Tissue Res 2012, 347, 245. [PubMed: 22006249]

[37]. Liu T, Wang X, Karsdal MA, Leeming DJ, Genovese F, Biomark Insights 2012, 7, 105. [PubMed: 22872786]

[38]. Seki E, De Minicis S, Gwak GY, Kluwe J, Inokuchi S, Bursill CA, Llovet JM, Brenner DA, Schwabe RF, J Clin Invest 2009, 119, 1858. [PubMed: 19603542]

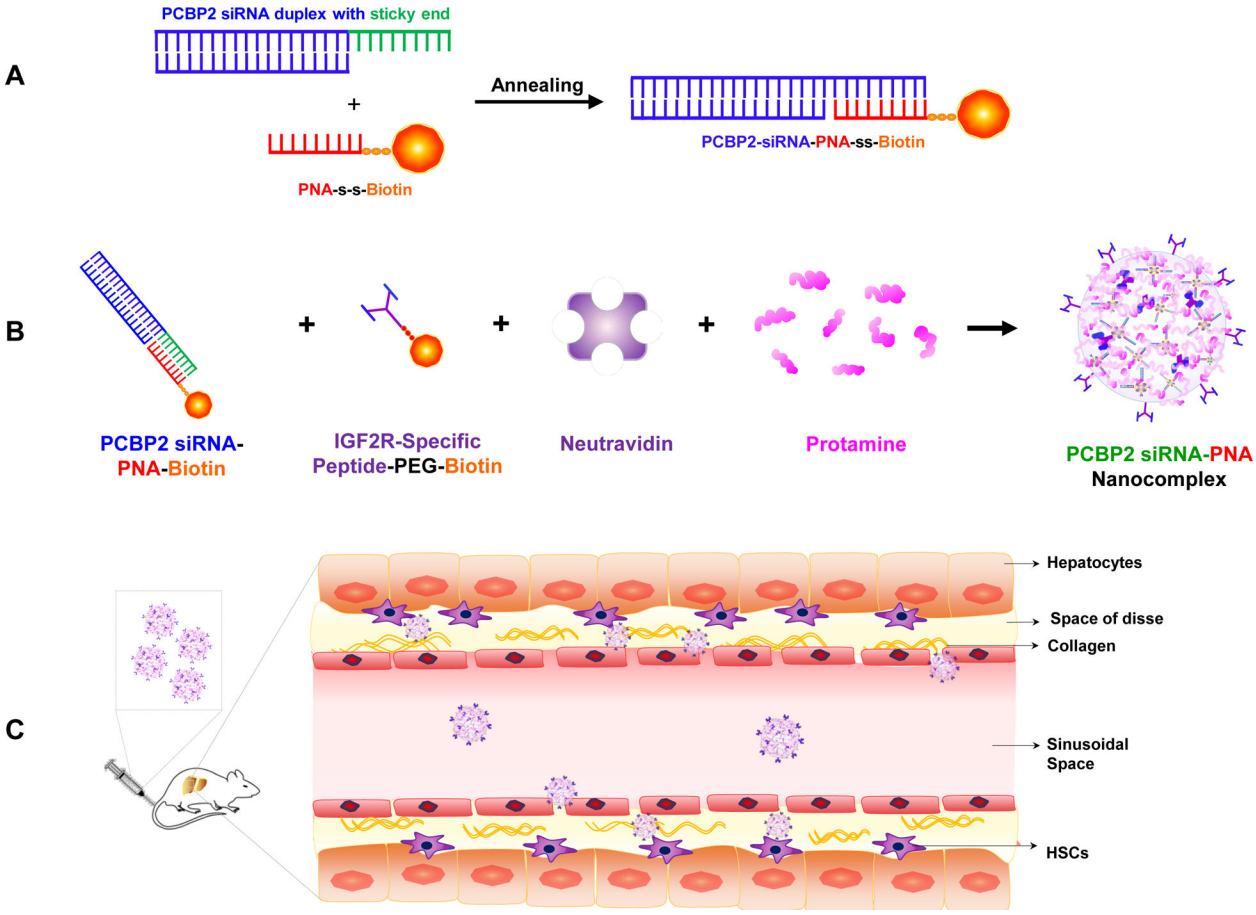

Figure 1. Schematics of the fabrication of the PCBP2 siRNA nanocomplex.

(A) Annealing of the PCBP2 siRNA to biotinylated PNA. (B) Fabrication of the PCBP2 siRNA nanocomplex. (C) Schematics of the delivery of the siRNA nanocomplex to HSCs after systematic administration.

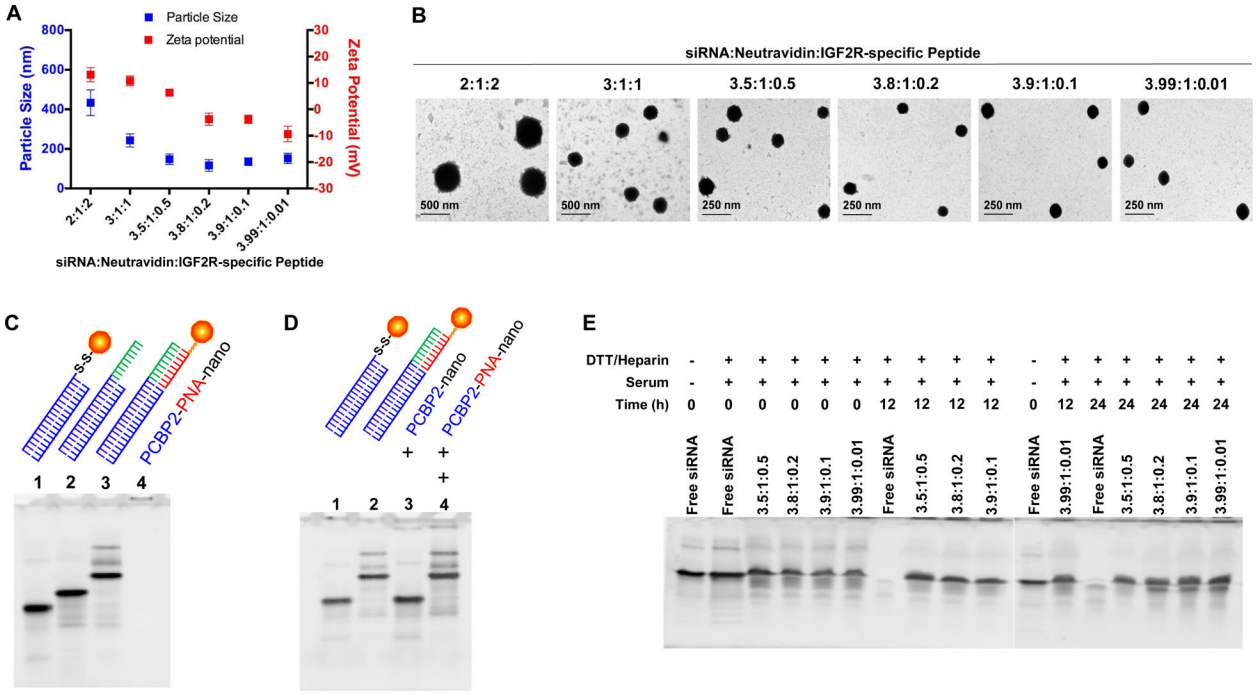

Figure 2. Characterization of the siRNA nanocomplexes with various siRNA:neutravitin:peptide molar ratios.

(A) Particle size and zeta potential of the siRNA nanocomplexes. (B) TEM of the siRNA nanocomplexes. (C) Gel retardation assay. Lane 1: Biotin-conjugated PCBP2 siRNA; Lane 2: PCBP2 siRNA with a sticky end at the 3' end of the sense strand; Lane 3: PCBP2 siRNA annealed with biotinylated PNA; Lane 4: PCBP2 siRNA nanocomplex containing the siRNA/PNA hybrid. (D) Release of siRNA after cleavage of disulfide bond by 100 mM DTT. Lane 1: Biotin-conjugated PCBP2 siRNA; Lane 2: PCBP2 siRNA annealed with biotinylated PNA; Lane 3: PCBP2 siRNA nanocomplex containing biotin-conjugated siRNA; Lane 4: PCBP2 siRNA nanocomplex containing the siRNA/PNA hybrid. (E) Serum stability of siRNA nanocomplexes. The nanocomplexes were incubated with 50% rat serum for 0, 12 and 24 h, followed by incubation with 40 μM heparin and 100 mM DTT to release intact siRNA.

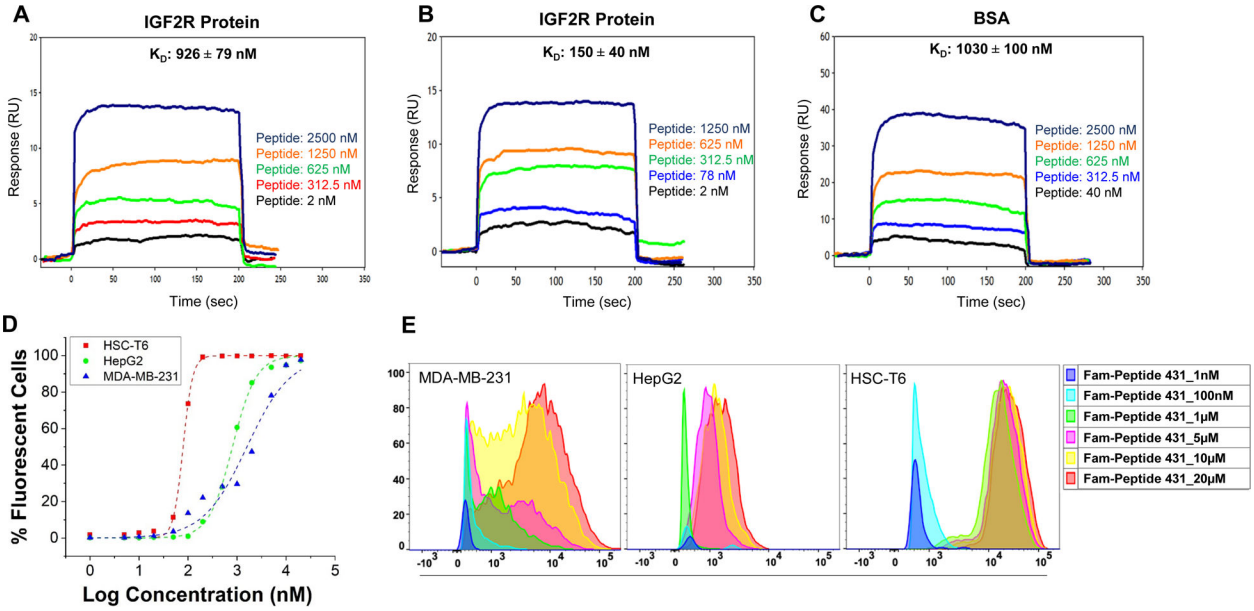

Figure 3. Affinity and specificity of dimeric peptie-431 to IGF2R.

(A) SPR sensograms of monomeric peptide-431 to human IGF2R protein; (B) SPR sensograms of dimeric peptide-431 to human IGF2R protein; (C) SPR sensograms of dimeric peptide-431 to BSA; (D) Binding curves of 5-FAM labeled dimeric peptide-431 to HSC-T6, HepG2, and MDA-MB-231 cells; (E) Flow cytometry histograms of the cells incubated with 5-FAM labeled dimeric peptide-431 at different concentrations.

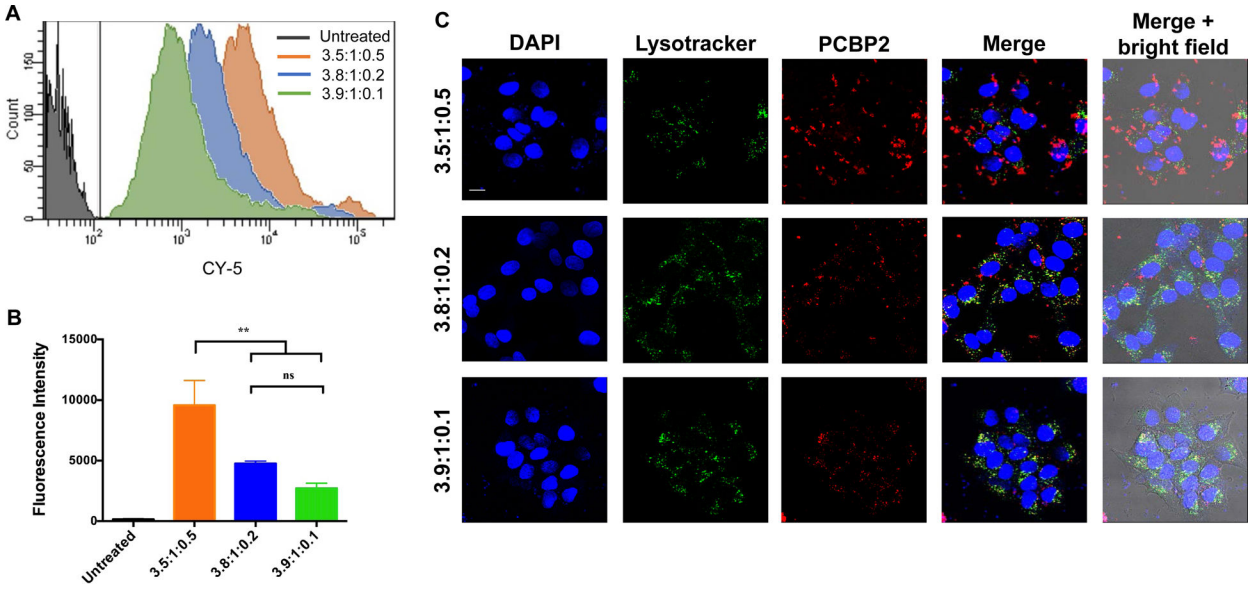

Figure 4. Cellular uptake of the siRNA nanocomplexes.

Cy5-labeled PCBP2 siRNA was encapsulated in nanocomplexes at different molar ratios (3.5:1:0.5, 3.8:1:0.2, 3.9:1:0.1) and incubated with HSC-T6 cells for 1 h. The cells were then analyzed with flow cytometry and confocal microscopy. (A) Flow cytometry histograms; (B) Fluorescence intensity; (C) Confocal imaging. Results are represented as the mean ± SD (n=5). ** represents $P<0.01$; ns represents no statistical significance.

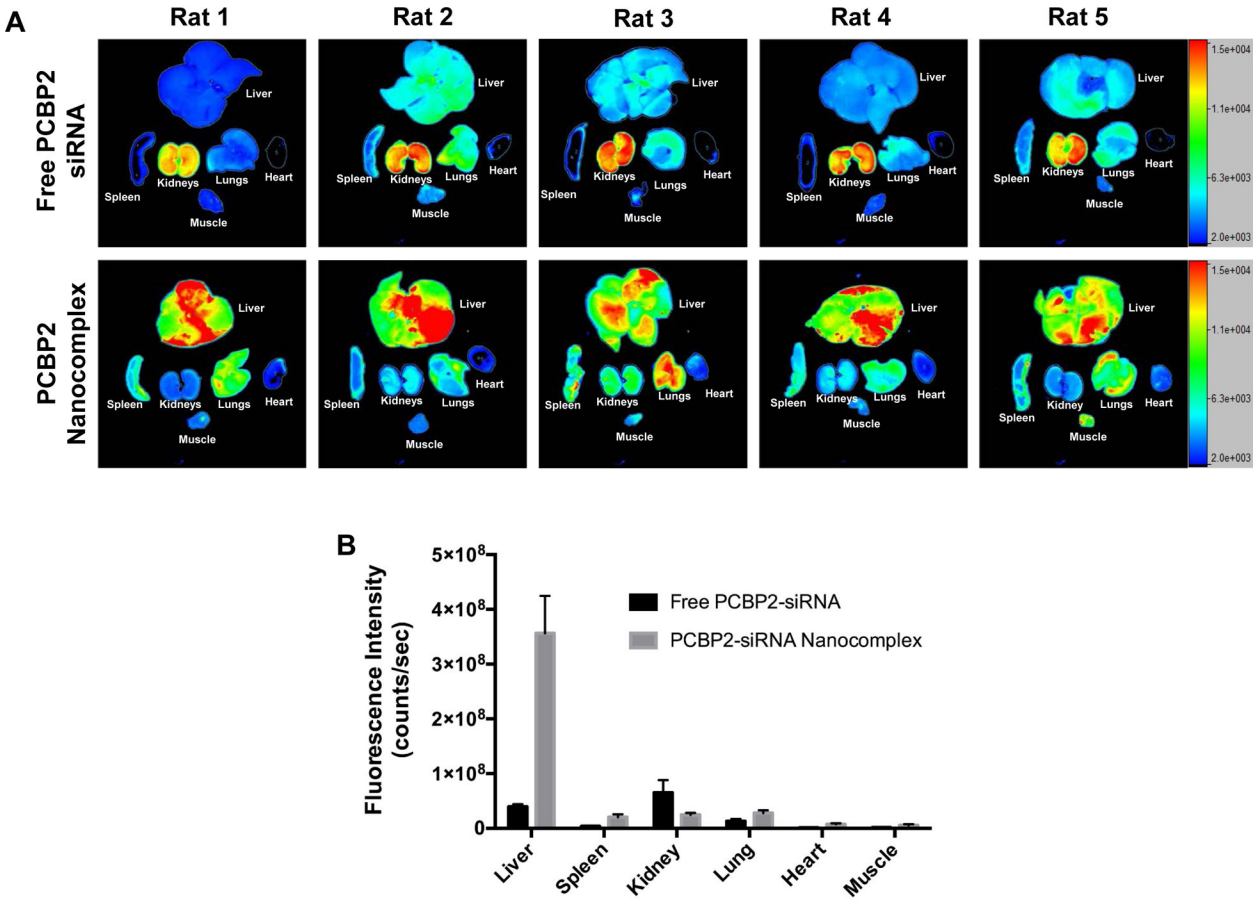

Figure 5. Biodistribution of the PCBP2 siRNA nanocomplex in rats with CCl_4-induced liver fibrosis.

One hour after injection of the Cy5-labeled siRNA nanocomplex (1 mg siRNA/kg) via tail vein, the rats were euthanized, and major organs including the liver, spleen, kidneys, lungs, heart and muscle were harvested for fluorescence analysis. (A) Fluorescence images of the harvested organs. (B) Fluorescence intensity of the harvested organs. Results are represented as the mean ± SD (n=5).

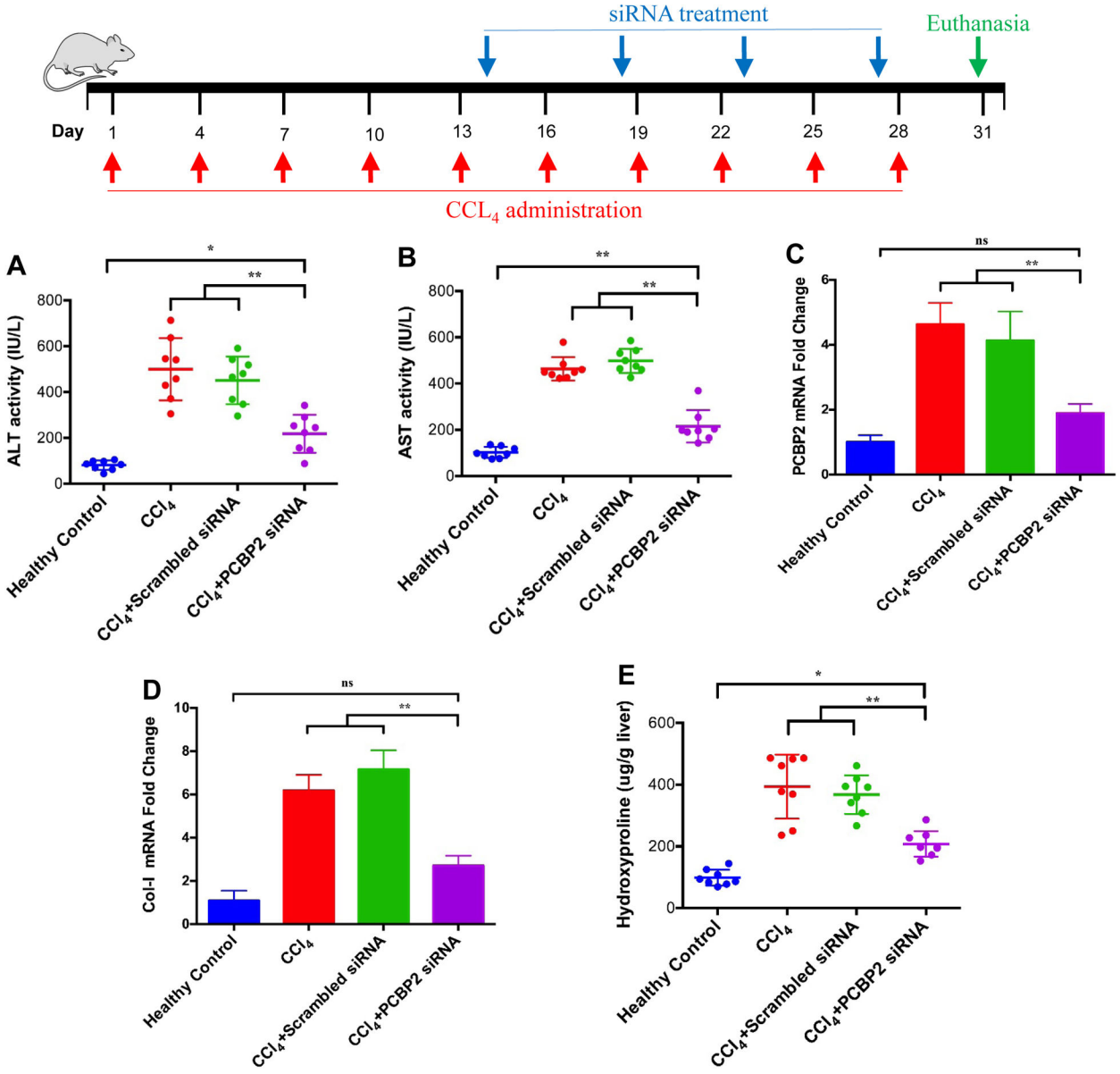

Figure 6. Anti-fibrotic activity study of the PCBP2 siRNA nanocomplex in rats with CCl_4-induced liver fibrosis.

The PCBP2 siRNA nanocomplex was administered at a dose of 1 mg/kg for four times. (A) Serum levels of ALT; (B) Serum levels of AST; (C) mRNA expression levels of PCBP2 in the liver; (D) mRNA expression levels of type I collagen in the liver; (E) Hydroxyproline content in the liver. (* $P < 0.01$; ** $P < 0.001$).

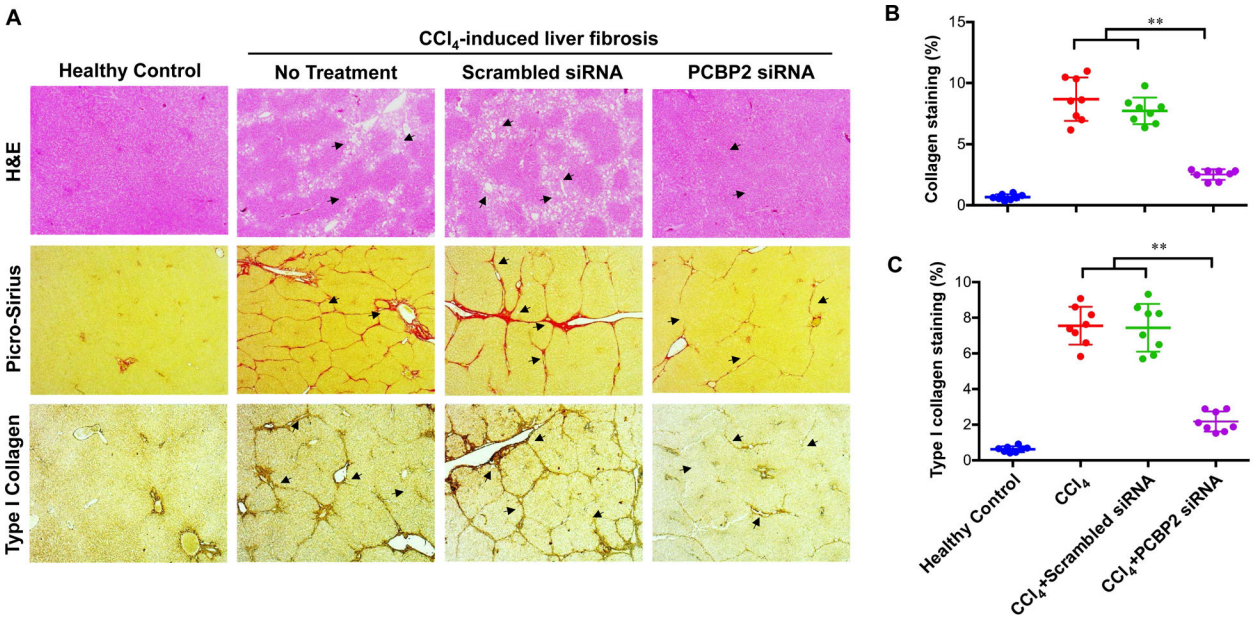

Figure 7. Histological analysis of liver specimen.

(A) H&E, Picro-Sirius Red, and type I collagen immunohistochemistry staining of liver specimen; (B) Picro-Sirius Red stained areas were quantified with ImageJ; (C) Type I collagen positive areas were quantified with ImageJ. (n=8) (** $p<0.01$)

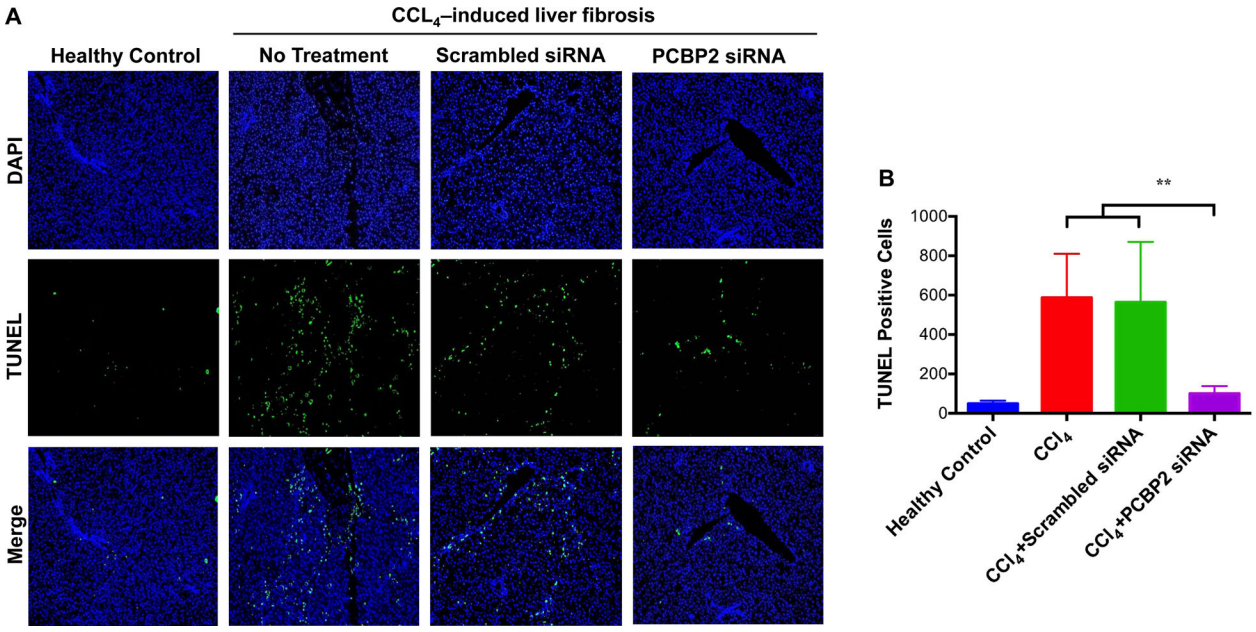

Figure 8. Effect of fibrosis resolution on hepatic apoptosis.

Hepatic apoptosis of liver specimen was evaluated with TUNEL assay. (A) Fluorescence images of live specimen; (B) Quantification of apoptotic cells with ImageJ. Results are represented as the mean ± SD (n=8) (** $p<0.01$)

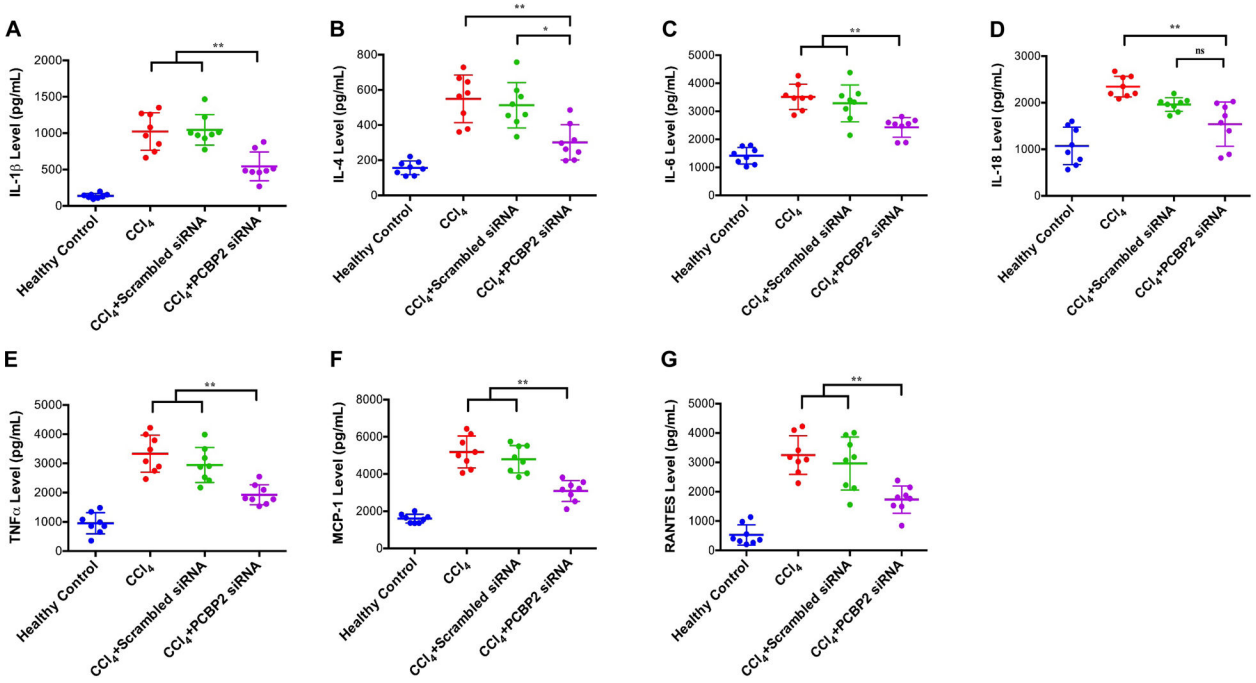

Figure 9. Serum levels of proinflammatory cytokines and chemokines.

(A) IL-1β; (B) IL-4; (C) IL-6; (D) IL-18; (E) TNFα; (F) MCP-1; (G) RANTES. Results are represented as the mean ± SD (n=8) (* $p<0.05$; ** $p<0.01$)